Magnetism in one-dimensional metamaterials: Double hyperbolic media and magnetic surface states

Georgia T. Papadakis[1,†], Dagny Fleischman[1,2], Artur Davoyan[1,2,3], Pochi Yeh[4], Harry A. Atwater[1]

[1]Thomas J. Watson Laboratories of Applied Physics, California Institute of Technology, California 91125, USA, [2]Kavli Nanoscience Institute, California Institute of Technology, California 91125, USA, [3]Resnick Sustainability Institute, California Institute of Technology, California 91125, USA, [4]Department of Electrical and Computer Engineering, University of Santa Barbara, California 93106, USA

[†]Corresponding author e-mail: gpapadak@caltech.edu

Abstract

Metamaterials with magnetic properties have been widely investigated with rather complex two- and three-dimensional resonant structures. Here we propose conceptually and demonstrate experimentally a mechanism for broadband optical magnetism in simpler one-dimensional systems. We experimentally demonstrate that alternating high-index dielectric/metal multilayer hyperbolic metamaterials can exhibit a strong magnetic response including variously $\mu > 1$ to $\mu < 0$. By engineering the electric permittivity as well, we reveal an epsilon and mu near zero regime. We show that modifications of internal metamaterial structure can lead to either type I or type II magnetic hyperbolic dispersion, thereby generalizing the notion of a hyperbolic metamaterial to encompass both TE and TM polarizations in simple multilayer geometries. Finally, we show that a negative magnetic response can give rise to TE interface-bound states, analogous to their TM counterparts, surface plasmon polaritons.

PACS numbers: 78.67.Pt, 73.20.Mf, 75.30.Gw, 78.20.Ls

Main Text and Figures

The interaction of matter with magnetic fields is usually described in terms of the magnetic permeability μ. In the optical regime, natural materials do not exhibit magnetic properties, as famously expressed in the textbook by Landau and Lifshitz[1]: "*there is no meaning in using the magnetic susceptibility from the optical frequencies onward, and in discussing such phenomena, we must put* $\mu = 1$". The lack of natural optical magnetism is associated with the weak magnetic coupling of the electromagnetic field with an atom, which is approximately 137 times weaker than the electric coupling[2]. Therefore, the magnetization of natural materials typically vanishes beyond frequencies in the GHz range. The critical parameters for engineering the magnetic response of materials are their internal electronic spin configuration, in the microscopic scale, and the induced currents they support when illuminated with electromagnetic fields, in the mesoscopic scale, in which metamaterials operate. The absence of natural magnetism at optical frequencies has motivated metamaterials researchers to seek for artificial structures exhibiting magnetic properties.

During the past decade, there have been numerous theoretical and experimental demonstrations of optical magnetism[3-13.] However up until now, the metamaterial structures that have been explored often require rather complex resonant geometries, for example arrays of paired thin metallic strips[6,7], split ring resonators[8] or fishnet structures[11]. Dielectric nanoparticles[14-16] and nanorods[12, 13] have been the building blocks

for three- and two-dimensional structures respectively (Fig. 1a, b). Apart from practical challenges in their experimental realization, resonant configurations are also limited in that their magnetic properties are narrowband in frequency.

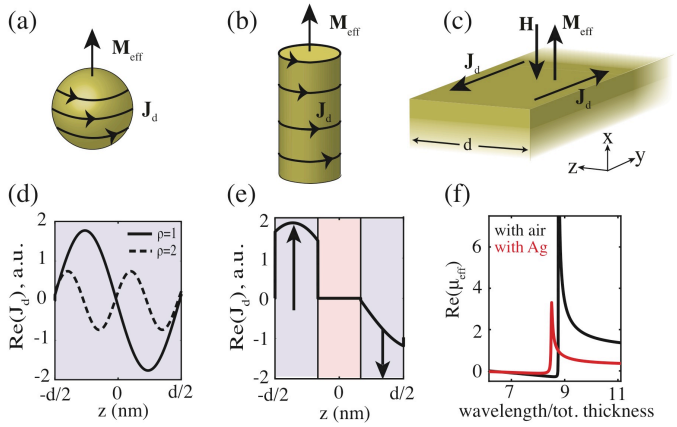

Fig.1. Induced magnetization in (a) dielectric nanoparticles (three-dimensional metamaterials) (b) in dielectric nanorods (two-dimensional metamaterials) and (c) in a one-dimensional dielectric slab. (d) Displacement current distribution at resonance, for $\rho = 1$ and $\rho = 2$ for a 90nm slab of refractive index $n_{diel} = 4.5$. (e) Displacement current distribution for two dielectric layers separated by air. (f) Effective permeability for two dielectric layers separated by air and Ag.

In this Letter, we demonstrate that one-dimensional metamaterials, which are easily experimentally realized by thin-film deposition, exhibit distinct and interesting magnetic properties. We start by considering a single subwavelength dielectric slab of refractive index n_{diel} and thickness d. When illuminated at normal incidence (z direction), its displacement current $\boldsymbol{J}_d = i\omega\varepsilon_o(n_{diel}^2 - 1)\boldsymbol{E}$ induces an effective magnetization $\boldsymbol{M}_{eff} = \tfrac{1}{2}\mu_o \int \boldsymbol{r} \times \boldsymbol{J}_d \cdot dS$ [1, 12, 17] (See Fig. 1c). By averaging the magnetic field $H_{avg} = \int_{-d/2}^{d/2} H(z)dz$ [18], we use $\mu_{eff} \approx 1 + M_{eff} / \mu_o H_{avg}$ to obtain an empirical closed form expression for the magnetic permeability:

$$\mu_{eff} \approx 1 - \frac{n_{diel}^2 - 1}{2n_{diel}^2}\left\{\frac{(n_{diel}\pi d/\lambda)}{tan(n_{diel}\pi d/\lambda)} - 1\right\} \qquad (1)$$

From Eq. (1), it is clear that the resonant behavior at free-space wavelengths $\lambda = n_{diel}d/\rho$, with $\rho = 1,2,...$ arises from anti-symmetric displacement current distributions, as shown in Fig. 1d, for $\rho = 1,2$. Eq. (1) serves to estimate the design parameters for enhanced magnetic response: in the metamaterials quasistatic limit $\lambda >> d$, only the fundamental and second resonance, $\lambda = n_{diel}d, n_{diel}d/2$ respectively, play significant roles. In the visible and near infrared regime, with layer thicknesses of the order [10-100] nm, dielectric indices higher than $n_{diel} = 2$ are required for obtaining strong magnetic effects. The displacement current distribution, closing a loop in $y = \pm\infty$, induces a magnetization $\boldsymbol{M}_{eff}$, which is opposite to the incoming magnetic field (Fig. 1c), leading to a diamagnetic response. The same principle applies for grazing incidence, with the displacement current inducing a magnetic response in the out-of-plane (z) direction.

Introducing a separation layer between high-index layers, as shown in Fig. 1e, enhances the magnetic response as dictated by $\boldsymbol{M}_{eff} \sim \boldsymbol{r} \times \boldsymbol{J}_d$, analogous to the two-dimensional case of a circular current with magnetic moment scaling with the disk surface area. This is demonstrated in Fig. 1f with μ_{eff} strongly

deviating from unity for both air and metallic separation. The nature of the intermediate layer does not play a crucial role as long as it does not introduce a significant additional component of current. Therefore, at optical frequencies, where the conductivity of metals ($\sim Im(\varepsilon_{metal})$) is small, metals do not significantly contribute to the magnetic response, in contrast to the GHz regime where the metallic component in resonant structures has been necessary for strong magnetic effects[6-8, 19, 20].

The magnetic permeability in Fig. 1f and in what follows is retrieved by taking the metamaterial finite thickness into account which allows decoupling the magnetic permeability from the electric permittivity[21]. In contrast, the extensively used effective medium approximations for layered media[22, 23] are unable to capture this magnetic response, as they are only appropriate for infinite periodic arrangements (See theoretical and experimental verification in Supplemental Material).

We now focus our attention on planar configurations with alternating metal and dielectric layers. Such heterostructures, termed "hyperbolic metamaterials" (HMMs), exhibit unprecedented light-matter interactions. Within the last couple of years, extraordinary properties have been reported, ranging from negative refraction[24-26] without the need of a negative refractive index, to diverging density of optical states[10,27] for Purcell-factor engineering[28] and hyper-lensing[29]. Describing HMMs with an effective permittivity tensor $\ddot{\varepsilon}_{eff} = \{\varepsilon_x = \varepsilon_o, \varepsilon_y = \varepsilon_o, \varepsilon_z = \varepsilon_e\}$, where the subscript-o (e) indicates the ordinary (extraordinary) direction, it can be shown that their unique features originate from their anisotropic electric response with $\varepsilon_o \varepsilon_e < 0$. The broadband nature and ease of fabrication makes HMMs the most promising metamaterial type in the optical-near infrared regime. Furthermore, similar to surface plasmonic waves at a dielectric-metal interface, HMMs support surface plasmonic-like modes attributed to the negative electric permittivity in their metallic components[30,31, 32].

Although both HMMs and natural plasmonic materials have featured prominently in photonics, up until now, their relevance has been limited to only transverse magnetic (TM) polarization fields, also termed electrically extraordinary waves due to electric field components in the plane of incidence. Planar HMMs have been thought to exhibit metallic behavior for transverse electric (TE) polarization (the magnetically extraordinary wave) because their magnetic properties have been assumed to be trivial and have thus remained unexplored. Furthermore, no TE counterpart of the surface plasmon polariton (SPP) has been reported at optical frequencies due to a lack of broadband negative magnetic response. In addition, artificial epsilon and mu near zero (EMNZ) metamaterials at optical frequencies are interesting building blocks for electrostatic-like electrodynamic systems that can achieve supercoupling between both magnetic and electric dipoles, due to a near zero phase advance in the material[33]. While it is straightforward to engineer the permittivity to cross zero in planar metamaterials[34], a simultaneously EMNZ metamaterial at optical frequencies has not yet been demonstrated. Being able to achieve unusual effective magnetic properties in planar structures may alleviate these limitations and has considerable potential to yield simple magnetic metamaterial designs at optical frequencies.

Figs. 1e, f indicate that high-index dielectric layers in planar hyperbolic metamaterials lead to strong magnetic effects. To demonstrate this, we first perform full-wave finite element simulations of Ag/dielectric multilayer metamaterials, where n_{diel} indicates the refractive index of the dielectric layer. The strong field localization in Fig. 2a inside the multilayer for $n_{diel} = 1.7$ and TM polarization is a consequence of the enhanced density of optical states due to the hyperbolic response with $\varepsilon_o \varepsilon_e < 0$[21, 28, 35,36]. The in-plane electric permittivity remains metallic-like ($\varepsilon_o < 0$) due to the presence of Ag, while the out-of plane permittivity is dielectric ($\varepsilon_e > 0$). By increasing the dielectric index ($n_{diel} = 4$) and switching the polarization state to TE,

we observe a similar hyperbolic behavior, shown in Fig. 2b. However, for TE polarization, light does not experience the permittivity anisotropy, therefore, the strong field localization cannot be attributed to a hyperbolic permittivity tensor. In order to explain this effect, we must introduce a tensorial magnetic permeability $\ddot{\mu}_{eff} = \{\mu_x = \mu_o, \mu_y = \mu_o, \mu_z = \mu_e\}$ which, together with $\ddot{\varepsilon}_{eff}$, fully describe the metamaterial. The TE field localization is a consequence of the $\mu_o\mu_e < 0$ condition.

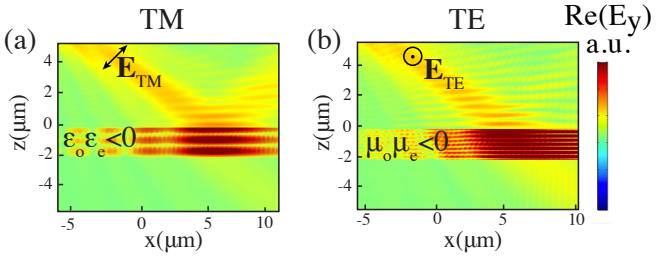

Fig.2 Simulation results for a dielectric/Ag multilayer metamaterial. Strong field localization is the consequence of (a) hyperbolic electric permittivity $\varepsilon_o\varepsilon_e < 0$ for $n_{diel} = 1.7$ and TM polarization and (b) hyperbolic magnetic permeability $\mu_o\mu_e < 0$ for $n_{diel} = 4$ and TE polarization

Artificially structuring the magnetic permeability along the ordinary and extraordinary axial directions can lead to wave propagation phenomena that are heretofore unexplored at optical frequencies. The scattering of TE polarized light from a uniaxial magnetic medium is described by: $\tan\vartheta = \tan\vartheta_{in} / \mu_o$ and $\tan\vartheta' = \tan\vartheta_{in} / \mu_e$, where ϑ and ϑ' are the refraction angle for phase and group velocity respectively. Therefore TE negative refraction of phase or energy can be demonstrated with negative magnetic response along the ordinary and extraordinary directions that correspond to magnetic hyperbolic dispersion of type II and I, respectively (Fig. 3a, b). With a near zero response along the ordinary direction, one can further access an EMNZ regime, for which light propagates without phase advance[33], as illustrated by the wave phase fronts in Fig. 3c. Considering surface wave propagation, we find that TE surface modes, with dispersion $\omega = kc\sqrt{\frac{1-\mu_o\mu_e}{\mu_e(\varepsilon_o - \mu_o)}}$, exist between air and a medium with negative magnetic response (Fig. 3d), analogous to the TM-polarized SPPs for negative electric permittivity.

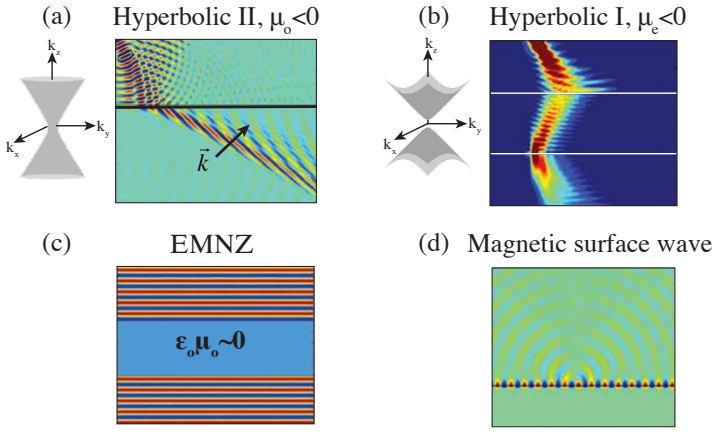

Fig.3: TE negative refraction of (a) phase and of (b) energy along with three-dimensional isofrequency diagrams for type II (a) and I (b) HMMs. (c) EMNZ propagation for $\mu_o, \varepsilon_o \sim 0$ (d) TE surface states

The permittivity and permeability values discussed in Fig. 3 can be achieved experimentally in one-dimensional metamaterials. We fabricated multilayer structures with electron-beam evaporation and first measured the optical constants of the individual constituent layers with spectroscopic ellipsometry, while we determined their thicknesses with transmission electron microscopy (TEM). We were thus able to homogenize the metamaterials by assigning them effective parameters $\ddot{\varepsilon}_{eff}$ and $\ddot{\mu}_{eff}$ using parameter retrieval methods[21], while also taking into account fabrication imperfections. We then performed ellipsometric measurements of the full metamaterial structures and we fitted the experimental data with the homogenization parameters ε_o, ε_e, μ_o and μ_e in a uniaxial model. The fitting was over-determined as the number of incident angles exceeded the total number of fitting parameters.

We first fabricated a Ge/Ag multilayer metamaterial (See TEM and schematic in Fig. 4d, inset). The germanium served as the high-index material for enhancing the magnetic resonance, while its absorption at optical frequencies contributed to broaden the magnetic response. For wavelengths larger than 800nm, the ordinary permeability μ_o is negative, while the extraordinary permeability μ_e remains positive (Fig. 4a). Therefore, this structure constitutes a type II magnetic hyperbolic metamaterial for TE polarization, as highlighted by the light-blue shading. Moreover, the presence of Ag induces a negative ordinary permittivity ε_o that becomes positive above 800nm due to the high-index of Ge (Fig. 4b). Thus, this metamaterial demonstrates an EMNZ response at optical frequencies. The agreement between fitting and experimental data is very good, as seen in Fig. 4c, d.

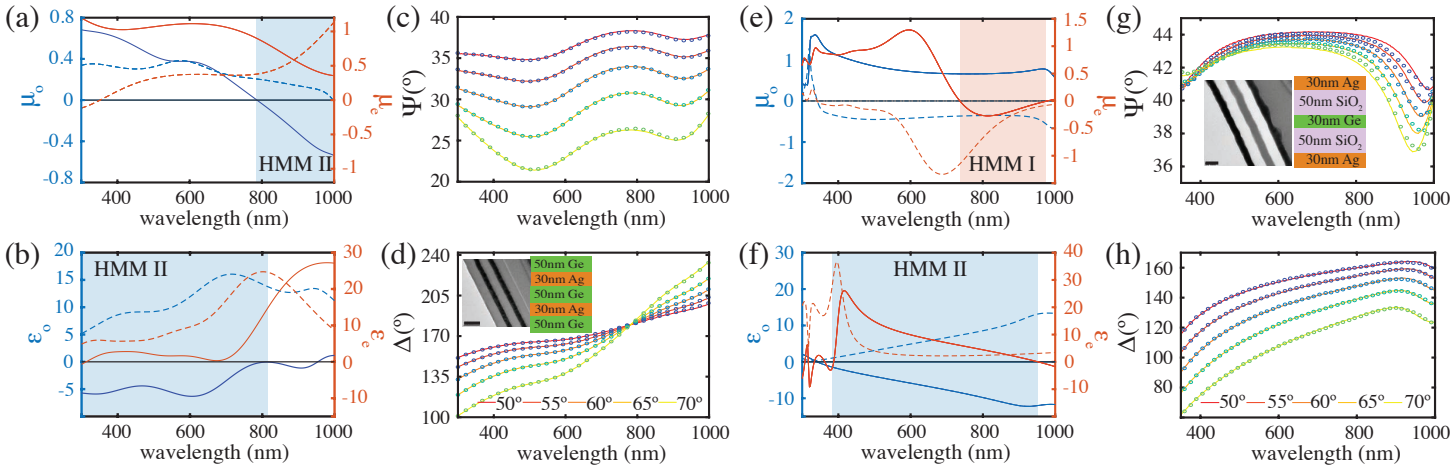

Fig.4: (a) Values for μ_o and μ_e fitted by ellipsometry (solid lines-real part, dashed lines-imaginary part), (b) ε_o and ε_e and (c), (d) agreement between experiment (solid lines) and magnetic model (circles) for an Ag /Ge HMM. (d) inset: schematic and TEM, scale bar: 100nm. (e) μ_o and μ_e, (f) ε_o and ε_e, (g), (h): Agreement between experiment and magnetic model for an Ag /SiO_2/Ge HMM. (g) inset: schematic and TEM, scale bar: 50nm.

Next, we explored a structure that supports type I magnetic hyperbolic dispersion ($\mu_e < 0$). Type I HMMs operating for TM polarization (with $\varepsilon_e < 0$), are of interest due to their significantly reduced losses compared to type II HMMs. Previously, broadband type I HMMs have only been realized with relatively complicated motifs composed of metallic nanowire arrays in a dielectric most[37]. However, it is possible in a one-dimensional layered structure to induce a negative magnetic response in the extraordinary direction; we break the periodicity of the multilayer while preserving mirror symmetry. Experimentally, we realized this concept with a Ag-SiO_2-Ge layered metamaterial, as shown in Fig. 4g (inset). The broken symmetry

introduces an anti-resonance in μ_e, yielding a type I magnetic TE-hyperbolic response above 730nm, highlighted by the light-orange shading in Fig. 4e. We obtain good agreement between the theoretical model and the experiment (Fig. 4g, h). We note that the negative imaginary parts of μ_o and μ_e arise from anti-resonances in their real parts to ensure Kramers-Kronig consistency and do not imply gain[21, 38].

We emphasize that these are metamaterials with an overall polarization-insensitive, *double* hyperbolic response. Specifically, apart from being hyperbolic for TE polarization, these heterostructures also exhibit a type II hyperbolic response for TM polarization with $\varepsilon_o < 0$ and $\varepsilon_e > 0$ (indicated in Figs. 4b, f with blue-shading).

Next, we study wave propagation of bulk and surface modes in multilayer structures that are simultaneously hyperbolic for both polarizations. We use a toy model consisting of five alternating layers of Ag and dielectric material with index n_{diel}, similar to the one studied experimentally (Figs. 4a-d). The metal/dielectric alteration leads to the TM hyperbolicity with $\varepsilon_o\varepsilon_e < 0$, while the high-index dielectric serves inducing a negative magnetic response and TE hyperbolic dispersion ($\mu_o\mu_e < 0$), as demonstrated in Fig. 4.

The interaction of radiative, bulk modes with the metamaterial is described in terms of isofrequency dispersion diagrams that indicate the wave-vector distribution and power flow. TE waves experience the magnetic anisotropy through $\frac{k_x^2 + k_y^2}{\varepsilon_o\mu_e} + \frac{k_z^2}{\varepsilon_o\mu_o} = \frac{\omega^2}{c^2}$, while the TM polarization depends on the electric permittivity anisotropy: $\frac{k_x^2 + k_y^2}{\varepsilon_e\mu_o} + \frac{k_z^2}{\varepsilon_o\mu_o} = \frac{\omega^2}{c^2}$. As seen in Fig. 5, the anisotropic magnetic response leads to TE hyperbolic isofrequency diagrams, revealing the possibility of propagation with unbound wavenumbers, negative refraction, enhanced Purcell effect, among numerous other phenomena (See Fig. 3). Up until now, these effects have only been reported for TM polarization, rising from electric permittivity anisotropies. Furthermore, we highlight the quantitatively similar response between TE and TM dispersion, not only for hyperbolic dispersion but also for elliptical dispersion when the metamaterial acts as an anisotropic dielectric (anisotropic magnetic medium) for TM (TE) polarization. The broad range of wavelengths for which we obtain similar dispersion for the two polarizations is indicative of the broadband nature of double hyperbolic metamaterials.

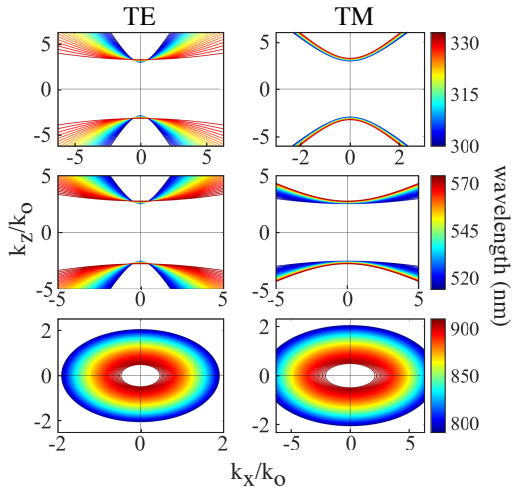

Fig.5: Isofrequency diagrams for a multilayer $n_{diel} = 4.5$ /Ag HMM for TE and TM polarization

Transverse magnetic surface plasmonic-like waves, at the interface between metal/dielectric metamaterials and air[31, 32], exhibit a characteristic dispersion that asymptotically approaches the surface plasmon frequency as shown in Fig. 6a, similar to typical SPPs on metallic interfaces[30, 39]. Such states are located at the interface between air and the metamaterial, with fields decaying away from the air/metamaterial boundary. In other words, they are located within the optical band gaps of both bounding media. These surface-bound modes can be found by identifying the eigenmodes of the metamaterial, through the mode condition of the transfer matrix $m_{11} = 0$ [40], which we implement numerically with the reflection pole method[41]. These plasmonic-like states are often interpreted in terms of a negative effective permittivity response[27,42], similar to typical SPPs on metallic surfaces. Indeed, this similarity is shown in Fig. 6c with the dotted and dashed curves, referring to SPPs on Ag and TM plasmonic waves on the multilayer shown in the background, respectively.

Performing the same analysis for TE polarization we find that TE polarized surface-bound plasmon-like modes also exist, when the metamaterial exhibits a negative effective magnetic response[42]. As shown in Fig. 6b, those states emerge at optical frequencies for dielectric layers with index $n_{diel} > 2$, in agreement with the empirical Eq. (1) and consistent with the negative magnetic response we discussed above. This confirms that these states can be seen as TE magnetic plasmons. Increasing the dielectric index redshifts the frequency regime for both TE and TM surface states (Figs. 6a, b). Similar to the bulk modes of Fig. 5, the surface states for TE and TM polarization also exhibit comparable propagation characteristics[43], as shown in Fig. 6c. This demonstrates the possibility of simultaneously exciting TM polarized plasmonic modes and also their TE polarized counterparts in metal/high-index-dielectric multilayers.

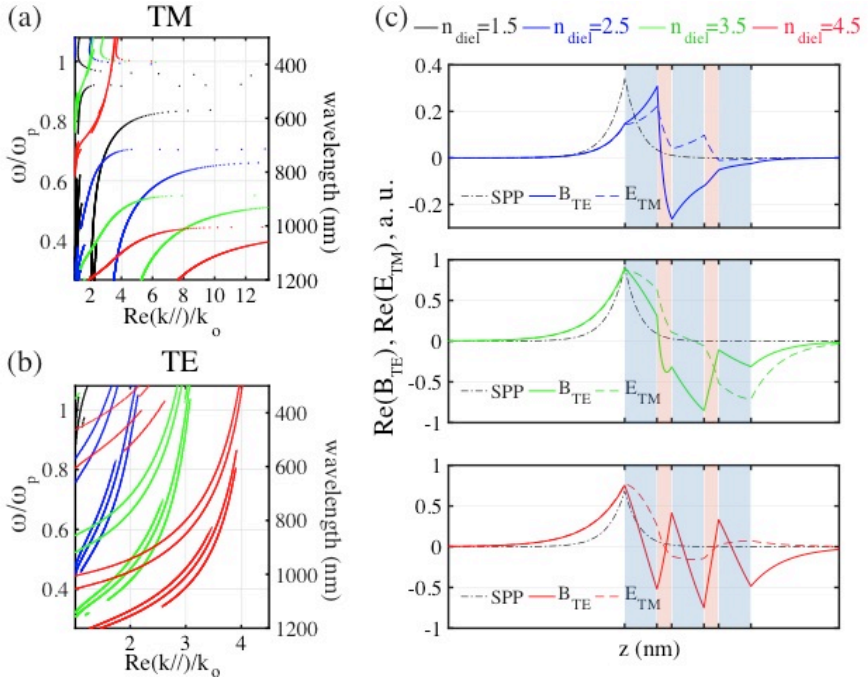

Fig.6: (a) TM dispersion characteristics of surface states for a n_{diel} /Ag multilayer, (b) TE dispersion. (c) Field profiles and comparison to SPP mode (black dotted line) on Ag. Black: $n_{diel} = 1.5$, blue: $n_{diel} = 2.5$, green: $n_{diel} = 3.5$, red: $n_{diel} = 4.5$: blue layers: dielectric, orange layers: Ag.

In conclusion, we have shown that non-trivial magnetic properties can be realized in one-dimensional

metamaterials, arising from displacement currents in dielectric regions. We have shown that it is possible to tailor the magnetic response of planar HMMs, which are typically explored based on their electric permittivity features. We experimentally demonstrated negative magnetic permeability in planar structures with magnetic hyperbolic dispersion, leading to type I and II *double* hyperbolic metamaterials. We have studied bulk and surface wave propagation and we have found that they exhibit a rather polarization-insensitive response. We report the existence of TE polarized 'magnetic plasmons', attributed to the negative effective magnetic permeability, which are complementary to the typical TM-polarized plasmon modes at the interface of negative permittivity materials. The results reported here can open a new direction for tailoring wave propagation in magnetic media in significantly simplified layered systems. We anticipate that these findings can enable the generalization of the unique properties of plasmonics and hyperbolic metamaterials, previously only explored for TM-polarized waves and negative permittivity media, for unpolarized light at optical frequencies.

This work was supported by U.S. Department of Energy (DOE) Office of Science grant DE-FG02-07ER46405 (G.P. and H.A.A.), and the Air Force Office of Scientific Research through MURI awards FA9550-12-1-0488 (D.F.) and FA9550-12-1-0024 (A.R.D.) G. T. Papadakis acknowledges support by the National Science Foundation Graduate Research Fellowship and the American Association of University Women Dissertation Fellowship. We acknowledge initial discussions with Dr. Krishnan Thyagarajan and fruitful feedback by Dr. Ragip Pala. We also thank Carol Garland and Barry Baker for assistance with sample preparation.

Supplemental Information

S I. New retrieval approach for multilayer metamaterials and comparison with effective medium theory and Bloch theory

The response of metal/dielectric multilayer hyperbolic metamaterials (HMMs) to transverse electric (TE) polarization is described through the dispersion equation for TE polarization: $\frac{k_x^2+k_y^2}{\varepsilon_o\mu_e}+\frac{k_z^2}{\varepsilon_o\mu_o}=\frac{\omega^2}{c^2}$. Traditionally, the electric permittivity has been approximated with the effective medium theory: $\varepsilon_o = f\varepsilon_{metal}+(1-f)\varepsilon_{diel.}$, $\varepsilon^{-1}{}_e = f/\varepsilon_{metal}+(1-f)/\varepsilon_{diel.}$, with ε_{metal} being the permittivity of the metal and $\varepsilon_{diel.}$ the permittivity of the dielectric while f is the metallic volume fraction. On the other hand, it has traditionally been assumed that since HMMs are composed of non-magnetic constituents materials, they must exhibit unity effective magnetic permeability, with $\mu_o = 1$ and $\mu_e = 1$. This has lead to the assumption that the TE response of planar HMMs is isotropic and metallic, while their effective magnetic properties have not been explored in the optical-infrared part of the spectrum. However, effective medium approximations (EMA) are only appropriate for unbound, i.e. infinite in size periodic arrangements[22, 23] – See Fig. S1a.

In the past decade, metamaterials with more complicated two- and three- dimensional subwavelength resonant elements have been homogenized with more rigorous parameter retrieval techniques that take into account the finite metamaterial thickness and decouple the magnetic permeability from the effective permittivity[44-47]. These approaches do not depend on the periodicity of the metamaterial, contrary to effective

medium approximations. We have recently shown[21] that, by generalizing this approach for multilayer hyperbolic media and treating them as effective slabs, and thus raising the constraint of an unbound effective medium, we are able to decouple the effective magnetic permeability from the electric permittivity along all coordinate directions and observe a local, broadband magnetic response for multilayer metamaterials composed of non-magnetic constituent materials. Those two different approaches: a) the EMA and Bloch theory and b) the effective slab approach are shown in Fig. S1a and b, respectively. Use of rigorous parameter retrieval techniques for oblique incidence also serves to justify the degree of locality of the effective parameters, contrary to assuming a priori local parameters based on the EMA.

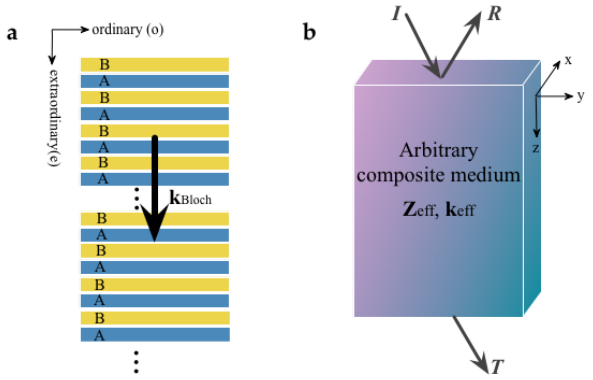

Fig. S1. (a) Unbound effective medium and Bloch homogenization approach. (b) effective slab approach.

The method in [21] accounts for the finite thickness of the multilayer metamaterial, by considering its transmission and reflection amplitudes. Knowing two scattering parameters: reflection and transmission, allows for calculation of two metamaterial parameters, namely, the effective impedance and wave-vector Z_{eff} and k_{eff}, respectively. These are decoupled through $Z_{eff} = k_{eff} / \varepsilon_{eff}$ and $k_{eff} = \mu_{eff} / Z_{eff}$, which lead to the separation of the electric and the magnetic responses of the metamaterial. Furthermore, considering the symmetry of the structure through the dispersion surfaces for the two polarizations: namely $\frac{k_x^2 + k_y^2}{\varepsilon_o \mu_e} + \frac{k_z^2}{\varepsilon_o \mu_o} = \frac{\omega^2}{c^2}$ for TE modes and $\frac{k_x^2 + k_y^2}{\varepsilon_e \mu_o} + \frac{k_z^2}{\varepsilon_o \mu_o} = \frac{\omega^2}{c^2}$ for TM modes respectively -in the case of planar structures-, leads to calculation of the effective permittivity tensor $\ddot{\varepsilon}_{eff} = (\varepsilon_o, \varepsilon_o, \varepsilon_e)$ and effective permeability tensor $\ddot{\mu}_{eff} = (\mu_o, \mu_o, \mu_e)$ discussed in the main text. To the contrary, both a) effective medium theories[22, 23] and b) Bloch wave-vector approaches[23, 48] account for an infinite A-B-type periodicity (See Fig. S1a), thus leaving no means of separating the electric from the magnetic response.

We show in Fig. S2 how the effective permittivities ε_o and ε_e of the effective slab approach[21], along both ordinary and extraordinary axial directions respectively, deviate both from the EMA (black line) and its non-local generalization (green line), which is based on the Bloch theory[23]. The imaginary parts of both ε_o and ε_e exhibit similar deviation from the EMA and Bloch approach as their real parts. The effective slab calculations pertain to a twenty-one layer metamaterial consisting of alternating SiO_2 and Ag layers. As can be seen in Fig. S2, the choice of the layer that terminates the overall heterostructure matters considerably: termination of the heterostructure with a metallic layer or a dielectric layer yield opposite trends in the effective electric permittivity response (See red and blue shaded areas in Fig. S2). Use of the finite effective slab retrieval[21] while setting a priori the magnetic permeability to unity yields results that coincide to the

EMA – See dashed blue and red lines in Fig. S2.

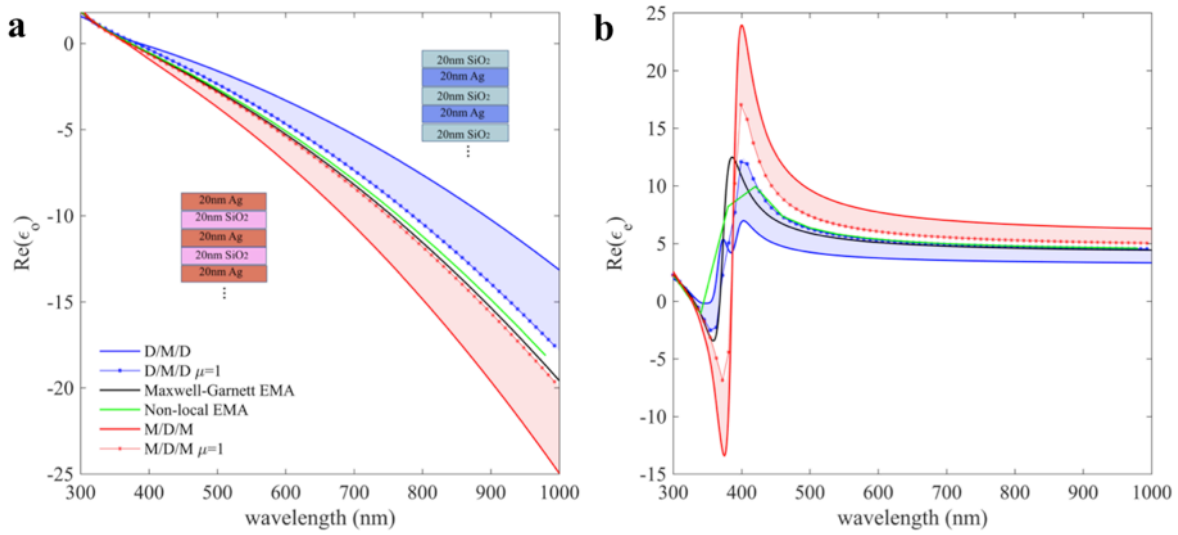

Fig. S2. Deviations of the effective slab approach, for 21 alternating layers of Ag and SiO_2, from the EMA (black line) and its non-local generalization (green). Terminating with dielectric (blue) and terminating with metal (red). (a) ordinary and (b) extraordinary directions

Although accounting for the finite thickness introduces corrections to the EMA and Bloch approaches, these corrections are small and still produce a qualitatively similar response in terms of electric permittivities ε_o and ε_e. However these corrections suffice to give a non-unity magnetic permeability tensor $\ddot{\mu}_{eff} = (\mu_o, \mu_o, \mu_e)$ shown in Fig. S3a. This tensor is local and the non-unity permeability is observed across the whole visible spectrum, contrary to previous resonant-based metamaterials[5-8].

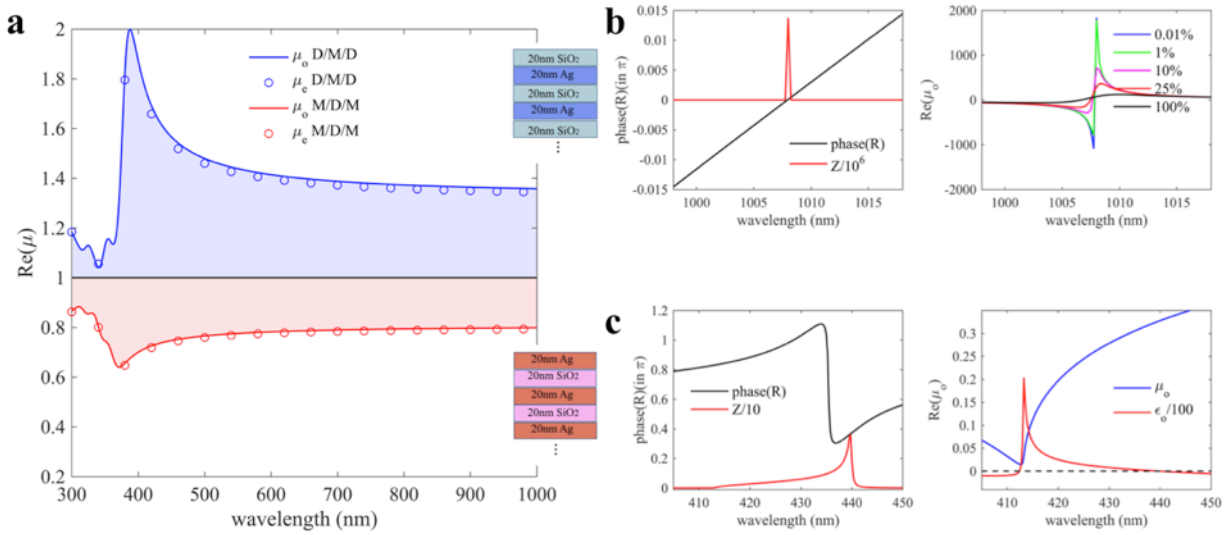

Fig. S3. (a) Layer-termination dependent effective magnetic permeability. (b) reflection phase, effective impedance (left) and effect of losses (right) (shown with legend in Fig S3b-right) for dielectric termination-PMC response. (c) reflection phase, effective impedance and electric and magnetic permeability for metallic termination-PEC response

The magnetic resonances shown in Fig. S3a are in agreement with Eq. (1) of the main text, where it is emphasized that, in order to obtain negative magnetic response at optical frequencies, refractive indices

higher $n_{diel} > 2$ are required, whereas here we used SiO_2, with $n_{SiO_2} \approx 1.5$. Additionally, the magnetic response in Fig. S3a is drastically different in the two cases of dielectric and metallic termination, yielding an effective isotropic paramagnetic and diamagnetic response respectively.

The resonance in magnetic permeability seen in Fig. S3a in the short wavelength regime can be associated to a perfect magnetic conductor (PMC) behavior (perfect electric conductor (PEC) behavior) when terminating the heterostructure with a dielectric (metal) layer. Specifically, dielectric layer termination yields a vanishing reflection phase at normal incidence - associated with a resonance in effective impedance (Fig. S3b, top-left). This is characteristic of a PMC with a vanishing magnetic field at the reflection interface.

In order to highlight the effect of losses, we first show qualitative results in Fig. S3b (top-right) for an Ag/SiO_2 structure in the lossless limit. The structure is terminated with SiO_2 and has magnified dimensions, in order to redshift the response and, thus, avoid confusion with the effects of interband transitions in Ag, in the small wavelength range. The magnetic permeability is resonant, as seen in Fig. S3b, right, in the lossless limit. However, turning on the metallic losses broadens the resonance, which transforms this effective magnetic response into a broadband one.

Equivalently, metallic termination yields a reflection phase of π and, thus, a PEC behavior with vanishing electric field at the reflection interface – see Fig. S3c. This results in a resonant electric permittivity that is accompanied with a near zero magnetic permeability, so that the product $\varepsilon \cdot \mu$ remains finite[38].

Hyperbolic metamaterial realizations with other dielectric materials like Al_2O_3 [36], LiF [49], TiO_2 [28] and other relatively low-index dielectrics in the visible part of the spectrum would be expected to exhibit a qualitatively similar behavior.

S II. Experimental Methods

We describe below the experimental approach taken for the samples discussed in the following section and in the main text. Our layered metamaterials were prepared by electron-beam evaporation onto Ge substrates (except the sample discussed in Fig. 4a-d of the main text, which was deposited on a Si substrate to avoid interface effects with the first Ge layer). All of the samples discussed in this work contain layers of 30nm of Ag and layers of 30nm-50nm of Ge and SiO_2. Each Ag layer was deposited by first seeding a 2nm AgO layer that is reduced to Ag under vacuum. This procedure was followed to obtain smoother Ag surfaces and interfaces. We found that following deposition of the first 2nm of smooth Ag, the remaining 28nm then yield far smoother surface and interfaces than if the Ag was deposited directly without using this process[50]. Atomic force microscopy (AFM) measurements indicated a Ag roughness of 2.13nm.

We characterize the optical properties of each constituent layer via spectroscopic ellipsometry on dummy samples and determine the exact thickness of each layer with transmission electron microscopy (TEM)– See Fig. S4. Thus, we are able to homogenize our metamaterials with the effective slab approach[21] (calculating $\varepsilon_o, \varepsilon_e, \mu_o, \mu_e$) and with the EMA[22] (calculating $\varepsilon_{o\mathrm{EMA}}, \varepsilon_{e\mathrm{EMA}}$) while taking into account fabrication and materials imperfections. Spectroscopic ellipsometry measurements were then taken on the metamaterials, for angles of incidence 50^o to 70^o with a step of 5^o. By taking measurements for five angles of incidence and fitting a) four effective parameters: $\varepsilon_o, \varepsilon_e, \mu_o, \mu_e$ in the effective slab model and b) two effective parameters: $\varepsilon_{o\mathrm{EMA}}, \varepsilon_{e\mathrm{EMA}}$ in the EMA model, the fitting problem is always over-determined. The ellipsometric fitting for all the samples discussed in this work was performed in the commercially available VASE system (J. A. Woollam Co.) and the effective parameters were all modeled with generalized Drude, Lorenz and Gaussian oscillators to ensure Kramers-Kronig consistency. The VASE system utilizes a Levenberg-Marquardt regression algorithm for the fit. We used the META6 model of WVASE to incorporate

the uniaxial anisotropy.

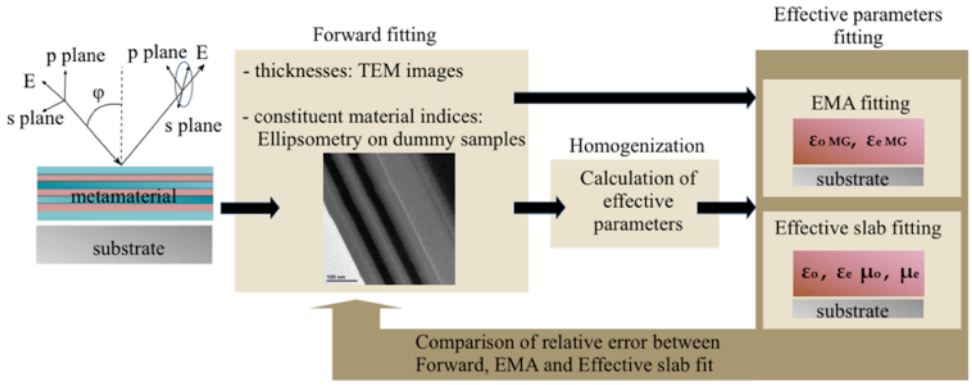

Fig. S4. Experimental approach with spectroscopic ellipsometry.

S III. Experimental verification of $\mu > 1$ and $\mu < 1$ and effective medium theory mismatch

In our first experiment, two samples of five alternating layers of 30nm Ag and 50nm SiO_2 were prepared onto Ge substrates, terminated with metallic and dielectric layers respectively. The schematics and TEM images of the samples are shown in the insets of Fig. S5a. Spectroscopic ellipsometry measurements were then taken for angles of incidence 50° to 70° with a step of 5° and two types of ellipsometric fittings were performed: one with the effective parameters ($\varepsilon_o, \varepsilon_e, \mu_o, \mu_e$) calculated through the effective magnetic slab approach[21], and one with the EMA ($\varepsilon_{o\text{EMA}}, \varepsilon_{e\text{EMA}}$). The sample with metallic termination exhibits a diamagnetic behavior ($\mu_o, \mu_e < 1$) while the dielectric terminated sample yields a paramagnetic response ($\mu_o, \mu_e > 1$), consistent with the results shown in Fig. S3 in Section S1.

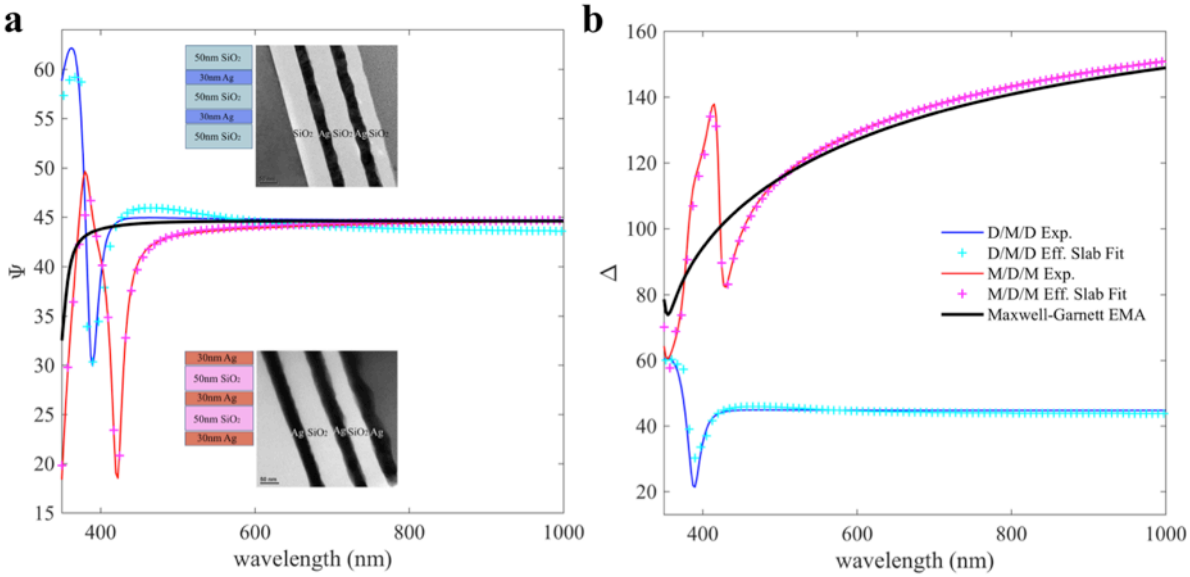

Fig. S5. Experimental-solid lines and fitted-crosses results for dielectric termination (blue/cyan) and metallic termination (red/magenta) for a five-layer 50nm SiO_2/ 30nm Ag metamaterial. Black line-EMA. Insets: schematics and TEM images.

As shown in Fig. S5a and b, the agreement of our effective magnetic slab approach with the experimental data is very good. The fitting results shown with cyan crosses correspond to an effective

paramagnetic response (see Fig. S3) when terminating the heterostructure with a dielectric layer, while the fitting results shown with magenta crosses correspond to an effective diamagnetic response (see Fig. S3), when terminating the heterostructure with a metal layer. In contrast to the good agreement that the magnetic model yields, the non-magnetic EMA model that describes for an infinite superlattice, fails to reproduce the experimentally measured resonant behavior of both Ψ and Δ in the small wavelength regime, where we observe a magnetic resonance, as shown in Fig. S5a, b with the black lines. We obtained qualitatevely similar agreement between experiment and effective magnetic slab approach for all angles of incidence.

S IV. Impedance matching

As discussed above, it is usually assumed that one-dimensional metamaterials composed of non-magnetic constituent materials do not exhibit magnetic properties. A complementary way to theoretically establish our findings, which contradict this assumption, is to perform an impedance-matching sanity check. We consider here a structure composed of the unit cell discussed in Fig. 1e-f of the main text, namely a stack of dielectric slabs with $n_{diel} = 4.5$ separated by air. We increase the number of layers to seventeen to increase the number of transmission peaks for which we perform the impedance matching. The impedance of this metamaterial is given by $Z_{magn.} = \sqrt{\frac{\mu_{eff}}{\varepsilon_{eff}}}$, where μ_{eff} and ε_{eff} are obtained through [21] for normal incidence. Setting a priori the effective magnetic permeability to unity: $\mu_{eff} = 1$ and performing the same homogenization yields different effective impedance $Z_{nonmagn.} = \sqrt{\frac{1}{\varepsilon_{eff,\mu=1}}}$. We emphasize that setting the magnetic permeability to unity in our effective-slab calculation through [21] is equivalent to using the effective medium theory results, as shown in Fig. S2 of Section SI: $\varepsilon_{EMA} \approx \varepsilon_{eff,\mu=1}$.

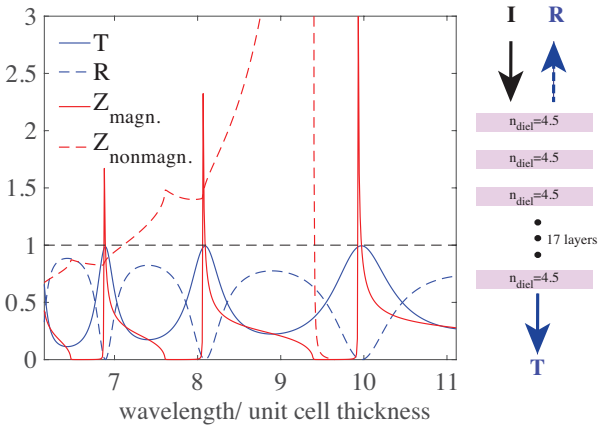

Fig. S6. Impedance matching condition for a seventeen-layers metamaterial composed of 30nm $n_{diel} = 4.5$ /30nm air alternating layers. The assumption of unity magnetic permeability fails to accurately predict the transmittance peaks.

It is clear from Fig. S6 that the non-magnetic model ($Z_{nonmagn.}$) fails to predict the transmittance peaks, as $Z_{nonmagn.}$ deviates from unity at the transmittance maxima. To the contrary, the magnetic model ($Z_{magn.}$) correctly crosses unity at the transmittance peaks. This indicates that it is necessary to account for an

effective magnetic permeability in describing wave propagation in one-dimensional metamaterials with finite thickness.

S V. Complementary to Figure 1f of the main text-Effective permittivities

In Fig. 1f of the main text we showed that the magnetic response of a layered metamaterials does not depend on the type of separation material between the high-index layers. Specifically, we showed that air and metallic (Ag) separation yield almost identical magnetic permeabilities due to the zero and relatively low current they support at optical frequencies, respectively. In contrast to the effective magnetic permeability, the effective permittivity ε_{eff} is drastically different in the two cases, as can be seen in Fig. S7. Specifically, the permittivity of the structure containing Ag becomes metallic in the long-wavelength regime, exhibiting Drude-like response similar to that of silver. On the other hand, the structure with air separation exhibits a dielectric response. These results are in qualitative agreement with the effective medium approximation.

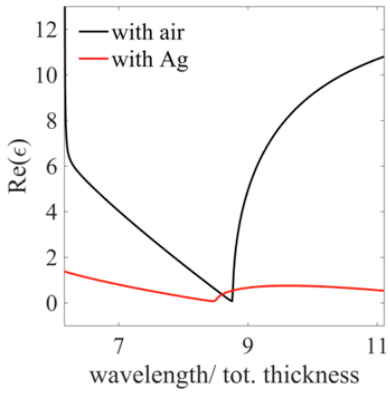

Fig. S7. Effective ε for two dielectric layers of $n_{diel} = 4.5$ separated by air and Ag, complementary to Fig. 1f in the main text

S VI. Ellipsometric fitting details, complementary to Fig. 4 of the main text

The ellipsometric fitting of the samples discussed in Fig. 4 of the main text was performed using the homogenized effective parameters $\ddot{\varepsilon} = diag(\varepsilon_o, \varepsilon_o, \varepsilon_e)$ and $\ddot{\mu} = diag(\mu_o, \mu_o, \mu_e)$, calculated through [21], as discussed in section S II. Apart from using the calculated effective parameters $\varepsilon_o, \varepsilon_e, \mu_o, \mu_e$ in a uniaxial homogeneous model to fit the experimental data discussed in the main text (Fig. 4), we also use the multilayer model, indicated as "forward fitting" in Fig. S4. This refers to the actual multilayer physical geometry of the samples, shown in the insets of Fig. 4d and 4g of the main text and in Fig. S8 below. We find that these two different types of models produce different relative error between model and experimental data, referred to -in ellipsometry terms- as normalized mean squared error (MSE). Specifically, we obtain increased MSE when modeling with the multilayer model (forward fitting), as compared to the effective slab fitting. This is consistent with and, in a sense, an experimental validation of the fact that the metamaterial is in the quasistatic limit: visible light does not experience the physical subwavelength multilayer structure but rather a quasi-homogeneous environment with electromagnetic properties described with the effective slab approach and the parameters $\varepsilon_o, \varepsilon_e, \mu_o, \mu_e$. A comparison of the two types of models is shown in Fig. S8, which refers to the results discussed in Fig. 4 of the main text.

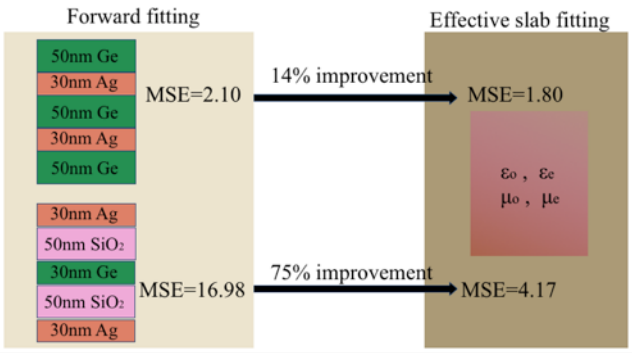

Fig.S8: Validity of quasistatic approximation for metal/high index dielectric HMMs discussed in Fig. 4 of the main text

The increased MSE observed for the structure containing SiO_2 is due to its smaller reflection amplitude, compared to the Ge/Ag one. Since the ellipsometric observables Ψ and Δ are based on the phase and amplitude of the reflection coefficient, more reflective samples are more appropriate for good experimental data extraction.

S VII. Polarization-insensitive HMMs – A Brewster angle approach

We demonstrated that use of high index materials, like germanium, incorporated in typical layered HMM geometries leads to magnetic resonances at visible wavelengths, attributed to strong circulating displacement current distributions (See Fig. 1 of the main text). The non-unity magnetic permeability, when negative, leads to TE hyperbolic bands, as shown in Fig. 5 of the main text. Complementary to those results and in order to systematically study these findings, we consider here, as in the main text, a HMM slab consisting of five alternating layers a dielectric material with index n_{diel} and silver. To highlight the main physical mechanism, we neglect the losses of silver. For the most common dielectric materials used to realize optical HMMs, like LiF, SiO_2 and Al_2O_3, the metamaterial behavior for TE polarized light is metallic, exhibiting a forbidden band across the visible range of frequencies, as shown, for example, in the reflectance spectrum for 45^o angle of incidence in Fig. S9a.

However, increasing the dielectric index introduces propagation bands within the band gaps as illustrated by the reflectance dips in Fig. S9a, for higher-index dielectrics (e.g. Si_3N_4 and TiO_2). Thus the typical isotropic metallic response for small n_{diel} (discussed in Section S1) is drastically altered to an extremely anisotropic response for larger n_{diel}, as shown in Fig. S9b. The strong angle-dependence of the TE reflectance spectrum resembles the typical anisotropic response of HMMs to TM polarization fields, which is usually interpreted in terms of a hyperbolic permittivity tensor.

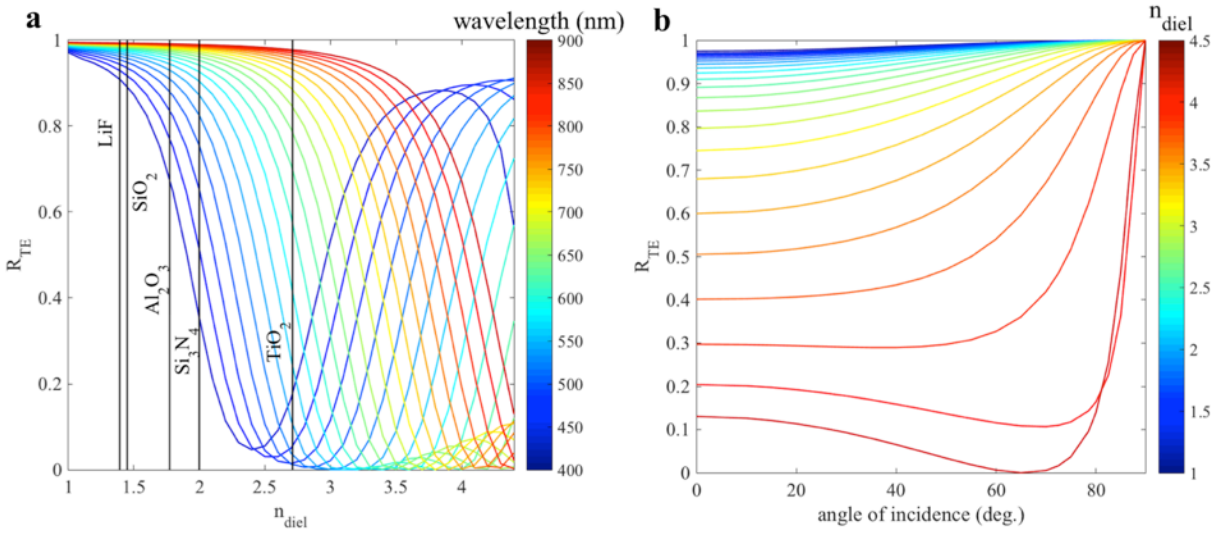

Fig.S9: a: TE Reflection spectra for a five layers n_{diel} /Ag HMM: propagation bands arise within the optical band gaps for high-enough dielectric index. b: Angle dependence of the reflectance at larger n_{diel} demonstrates the hyperbolic response to TE polarization at the wavelength of 600nm

The reflectance null near 65 degrees incidence angle in Fig. S9b can be interpreted as the Brewster angle for TE polarization in planar magnetic HMMs, due to its striking resemblance to the well-known Brewster angle that occurs in dielectric media with non-unity electric permittivity ($\tan\theta_B = \sqrt{\varepsilon}$) for TM polarization[51]. This is a complementary means of validating a non-unity magnetic permeability, without using a retrieval approach.

Thus, the TE propagating bands depicted in Fig. S9a for high-n_{diel} HMMs and the negative effective magnetic permeability seen in the main text are interrelated. These propagating bands are hyperbolic bands. This is demonstrated in Fig. 5 of the main text, where, by performing the effective slab homogenization[21], we presented the isofrequency diagrams for a $n_{diel} = 4.5$ /Ag HMM for both polarizations. The TE dispersion surface, which depends on the effective magnetic permeability through $\frac{k_x^2 + k_y^2}{\varepsilon_o \mu_e} + \frac{k_z^2}{\varepsilon_o \mu_o} = k_o^2$, opens up into a hyperboloid in frequency regimes with $\mu_o \mu_e < 0$.

These findings can be generalized to any dielectric index that is high enough to introduce propagation bands within the band gap of the metamaterial (Fig. S9a) for TE polarization and, thus, an extremely anisotropic response.

S VIII. TE magnetic surface states

In the main text, we examine the surface states of finite-thickness dielectric/Ag heterostructures. For the structures considered (five alternating layers of dielectric: 55nm/Ag: 25nm), we display in Fig. S10 their extracted effective magnetic permeabilities.

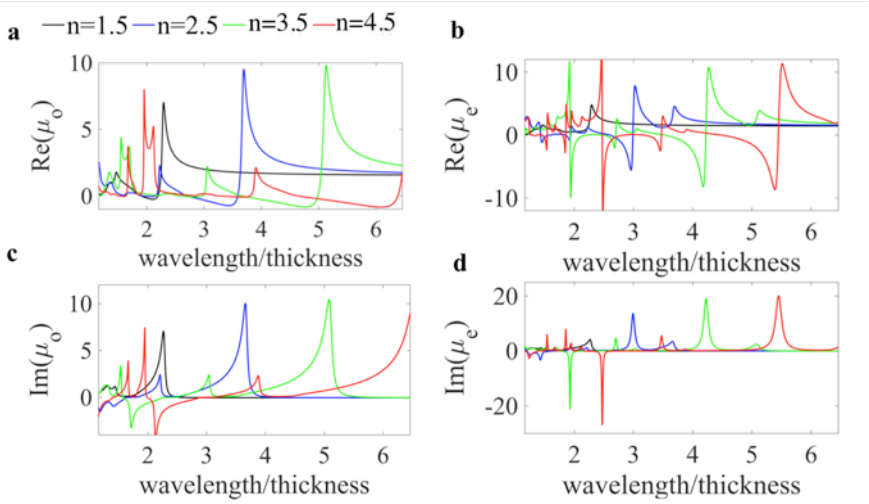

Fig.S10: Dielectric index-dependence of the effective permeability for a planar dielectric/Ag structure of five alternating layers: dielectric: 55nm/Ag: 25nm.

For dielectric materials with $n_{diel} < 2$, the resonances of both μ_o and μ_e and, thus, the negative magnetic response is located near the UV spectral range. However as the dielectric index increases, the magnetic response becomes stronger and the wavelength regime of negative effective permeability regime red-shifts to visible and near infrared wavelengths. This red-shifting of the negative magnetic response with increasing dielectric index shown in Fig. S10, in turn, leads to red-shift of the TE magnetic surface states, as shown in Fig. 6b of the main text. Specifically, as pointed out in the main text, the wavelengths at which we identify surface states coincide with the wavelengths for which the magnetic surface wave dispersion $\omega = kc\sqrt{\dfrac{1-\mu_o\mu_e}{\mu_e(\varepsilon_o-\mu_o)}}$ is satisfied.

For completeness, we present in Fig. S11 the corresponding effective electric permittivity for the metamaterials discussed here.

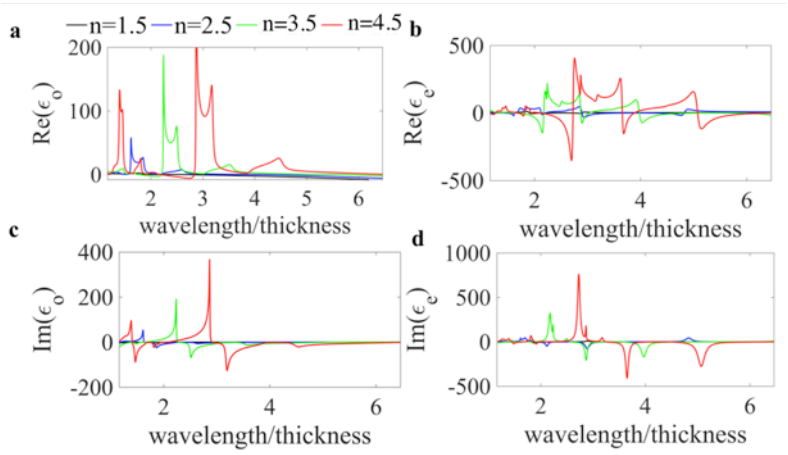

Fig.S11: Dielectric index-dependence of the effective permittivity for a planar dielectric/Ag structure of five alternating layers: dielectric: 55nm/Ag: 25nm.

The in-plane ordinary permittivity ε_o exhibits a metallic-like negative response in the long-

wavelength regime, which is responsible for the SPP-like surface states reported in the main text, Fig. 6a, for TM polarization. Similarly to the magnetic permeability discussed above, an increase in the dielectric index leads to a red-shift of this negative response of ε_o, which translates to red-shifting of the TM-SPP surface states dispersion, as shown in Fig. 6a of the main text. As pointed out in the main text, negative imaginary values for all the constitutive parameters ε_o, ε_o, μ_o and μ_e arise from anti-resonances in their real parts[38] to ensure Kramers-Kronig consistency, and do not imply gain.

Finally, we display numerical results for the propagation decay length of both TE and TM plasmonic-like modes in Fig. S12, complementary to Fig. 6 in the main text. The two surface states have similar decay lengths. This is consistent with Fig. 6c of the main text where we demonstrated that the two surface states have similar field distributions.

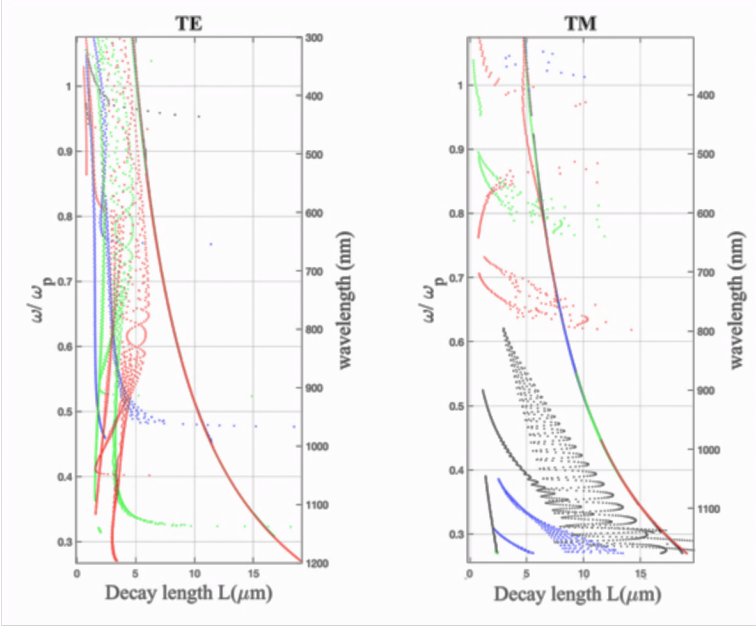

Fig.S12: Decay length of TE and TM surface states at the interface between air and a planar dielectric/Ag structures of five alternating layers: dielectric: 55nm/Ag: 25nm. Dielectric index is: 1.5 for black, 2.5 for blue, 3.5 for green and 4.5 for red.

References

1 L. D. Landau, E. M. Lifshitz, and L. P. Pitaevskii, *Electrodynamics of Continuous Media*, 1984).

2 F. Monticone and A. Alù, Journal of Materials Chemistry C **2**, 9059 (2014).

3 D. Schurig, J. J. Mock, B. J. Justice, S. A. Cummer, J. B. Pendry, A. F. Starr, and D. R. Smith, Science **314**, 977 (2006).

4 D. R. Smith, W. J. Padilla, D. C. Vier, S. C. Nemat-Nasser, and S. Schultz, Physical Review Letters **84**, 4184 (2000).

5 S. Linden, C. Enkrich, M. Wegener, J. Zhou, T. Koschny, and C. M. Soukoulis, Science **306**, 1351 (2004).

6 S. Gennady and A. U. Yaroslav, Journal of Optics A: Pure and Applied Optics **8**, S122 (2006).

7 U. K. Chettiar, A. V. Kildishev, T. A. Klar, and V. M. Shalaev, Opt. Express **14**, 7872 (2006).

[8] J. Zhou, T. Koschny, M. Kafesaki, E. N. Economou, J. B. Pendry, and C. M. Soukoulis, Physical Review Letters **95**, 223902 (2005).
[9] J. B. Pendry, Physical Review Letters **85**, 3966 (2000).
[10] A. B. Evlyukhin, S. M. Novikov, U. Zywietz, R. L. Eriksen, C. Reinhardt, S. I. Bozhevolnyi, and B. N. Chichkov, Nano Letters **12**, 3749 (2012).
[11] S. S. Kruk, Z. J. Wong, E. Pshenay-Severin, K. O'Brien, D. N. Neshev, Y. S. Kivshar, and X. Zhang, Nat Commun **7** (2016).
[12] M. S. Mirmoosa, S. Y. Kosulnikov, and C. R. Simovski, arXiv.org (2016).
[13] O. B. Stephen and B. P. John, Journal of Physics: Condensed Matter **14**, 4035 (2002).
[14] N. Engheta, A. Salandrino, and A. Alù, Physical Review Letters **95**, 095504 (2005).
[15] H. Alaeian and J. A. Dionne, Opt. Express **20**, 15781 (2012).
[16] A. I. Kuznetsov, A. E. Miroshnichenko, Y. H. Fu, J. Zhang, and B. Luk'yanchuk, Scientific Reports **2**, 492 (2012).
[17] J. B. Pendry and D. R. Smith, Physics Today **57** (2004).
[18] D. R. Smith and J. B. Pendry, Journal of the Optical Society of America B **23**, 391 (2006).
[19] R. S. Penciu, K. Aydin, M. Kafesaki, T. Koschny, E. Ozbay, E. N. Economou, and C. M. Soukoulis, Opt. Express **16**, 18131 (2008).
[20] L. Langguth and H. Giessen, Opt. Express **19**, 22156 (2011).
[21] G. T. Papadakis, P. Yeh, and H. A. Atwater, Physical Review B **91**, 155406 (2015).
[22] V. Agranovich and V. Kravtsov, Solid State Communications **55**, 85 (1985).
[23] X. Ni, S. Ishii, M. D. Thoreson, V. M. Shalaev, S. Han, S. Lee, and A. V. Kildishev, Opt. Express **19**, 25242 (2011).
[24] A. A. High, R. C. Devlin, A. Dibos, M. Polking, D. S. Wild, J. Perczel, N. P. de Leon, M. D. Lukin, and H. Park, Nature **522**, 192 (2015).
[25] A. Poddubny, I. Iorsh, P. Belov, and Y. Kivshar, Nat Photon **7**, 948 (2013).
[26] E. Verhagen, R. de Waele, L. Kuipers, and A. Polman, Physical Review Letters **105**, 223901 (2010).
[27] E. E. Narimanov, Physical Review X **4**, 041014 (2014).
[28] H. N. S. Krishnamoorthy, Z. Jacob, E. Narimanov, I. Kretzschmar, and V. M. Menon, Science **336**, 205 (2012).
[29] D. Lu and Z. Liu, Nat Commun **3**, 1205 (2012).
[30] S. A. Maier and H. A. Atwater, Journal of Applied Physics **98**, 011101 (2005).
[31] H. J. Lezec, J. A. Dionne, and H. A. Atwater, Science **316**, 430 (2007).
[32] J. A. Dionne, E. Verhagen, A. Polman, and H. A. Atwater, Opt. Express **16**, 19001 (2008).
[33] A. M. Mahmoud and N. Engheta, Nat Commun **5** (2014).
[34] R. Maas, J. Parsons, N. Engheta, and A. Polman, Nat Photon **7**, 907 (2013).
[35] V. P. Drachev, V. A. Podolskiy, and A. V. Kildishev, Opt. Express **21**, 15048 (2013).
[36] Z. Jacob, J.-Y. Kim, G. V. Naik, A. Boltasseva, E. E. Narimanov, and V. M. Shalaev, Appl. Phys. B **100**, 215 (2010).
[37] Y. Guo, W. Newman, C. L. Cortes, and Z. Jacob, Advances in OptoElectronics **2012**, 9 (2012).
[38] T. Koschny, P. Markoš, D. R. Smith, and C. M. Soukoulis, Physical Review E **68**, 065602 (2003).
[39] E. N. Economou, Physical Review **182**, 539 (1969).
[40] P. Yeh, *Optical Wave in Layered Media* (Wiley, Hoboken, NJ, 1988).

[41] E. Anemogiannis, E. N. Glytsis, and T. K. Gaylord, Journal of Lightwave Technology **17**, 929 (1999).
[42] A. P. Vinogradov, A. V. Dorofeenko, S. G. Erokhin, M. Inoue, A. A. Lisyansky, A. M. Merzlikin, and A. B. Granovsky, Physical Review B **74**, 045128 (2006).
[43] Z. Sun, X. Zuo, T. Guan, and W. Chen, Opt. Express **22**, 4714 (2014).
[44] D. R. Smith, D. C. Vier, T. Koschny, and C. M. Soukoulis, Physical Review E **71**, 036617 (2005).
[45] D. R. Smith, S. Schultz, P. Markoš, and C. M. Soukoulis, Physical Review B **65**, 195104 (2002).
[46] X. Chen, T. M. Grzegorczyk, B.-I. Wu, J. Pacheco, and J. A. Kong, Physical Review E **70**, 016608 (2004).
[47] Y. Minowa, T. Fujii, M. Nagai, T. Ochiai, K. Sakoda, K. Hirao, and K. Tanaka, Opt. Express **16**, 4785 (2008).
[48] P. Yeh, *Optical waves in layered media* (John Wiley & Sons, Hoboken, New Jersey, 1988).
[49] T. Tumkur, G. Zhu, P. Black, Y. A. Barnakov, C. E. Bonner, and M. A. Noginov, Applied Physics Letters **99**, 151115 (2011).
[50] K. Thyagarajan, C. Santschi, P. Langlet, and O. J. F. Martin, Advanced Optical Materials, n/a (2016).
[51] R. Watanabe, M. Iwanaga, and T. Ishihara, physica status solidi (b) **245**, 2696 (2008).